Electronic Supplementary Material (ESI) for Green Chemistry.

Supplementary Information

Lithium-mediated Ammonia Synthesis from Water and Nitrogen: A Membrane-free Approach Enabled by Immiscible Aqueous/Organic Hybrid Electrolyte System

Kwiyong Kim[‡§], Yifu Chen[‡], Jong-In Han, Hyung Chul Yoon and Wenzhen Li[*]

Table of Contents

1. Experimental methods

1.1. Materials

Lithium perchlorate ($LiClO_4$, battery grade, 99.99% trace metal basis), propylene carbonate (PC, $C_4H_6O_3$, 99.7 %), poly(methyl methacrylate) (PMMA, $[CH_2C(CH_3)(CO_2CH_3)]_n$, average $M_w \sim 15{,}000$), 2-methyltetrahydrofuran (2Me-THF, $C_5H_{10}O$, 99.7 %), sodium salicylate ($C_7H_5NaO_3$), sodium hydroxide (NaOH), sodium nitroferricyanide dihydrate ($Na_2[Fe(CN)_5NO]\cdot 2H_2O$), sodium hypochlorite solution (NaOCl, available chlorine 4.00-4.99 %), and nickel foil (Ni, thickness: 0.1 mm, 99.98 %) were all purchased from Sigma-Aldrich. Sulfuric acid (H_2SO_4, trace metal grade) was obtained from Alfa Aesar. Ammonia standard solution (NH_3-N, 100 mg L^{-1}) was purchased from Hach.

1.2. Design of electrochemical system

Preparation of electrodes: Ni substrate, a cathode for Li deposition, was prepared by cutting Ni foil into a dimension of 0.5 cm × 1.5 cm. Then, the back side of the foil was pasted on electrical tape. The actual working area of Li deposition, immersed in an organic electrolyte, was 0.25 cm^2. Platinum wire served as an anode during Li deposition. A Platinum wire was a pseudo-reference electrode. All the potentials in this work are referenced to the Li^+/Li electrode potential, obtained by calibration of the reference electrode against a fresh Li metal before the experiment (0 V vs. Li^+/Li corresponds to -3.20 ± 0.05 V vs. Pt wire).[1]

Preparation of electrolytes and electrolytic cell: Different amounts of PMMA, with mass concentrations of 0, 1, 2 and 3 wt.%, were dissolved in a pristine electrolyte of 1 M $LiClO_4$ in PC. Thus prepared PC-based electrolytes served as an organic catholyte for Li deposition. 1 M $LiClO_4$ aqueous solution was used as anolyte in which oxygen evolution reaction (OER) occurred. Note that, as shown in Figure 2(a), since the density of PC is higher than that of water (ρ_{PC} = 1.2 g cm^{-3} vs. ρ_{water} = 0.997 g cm^{-3}), the aqueous phase floats on top of the organic electrolyte. Reactions were performed in an electrochemical cell made using a three-neck flask (Figure S1). We designed our electrolytic cell to include an internal cylindrical wall which surrounds the floating aqueous electrolyte and anode, thereby mitigating excessive interfacial diffusion of water into the organic phase, as shown in Figure S1. The

electrochemical reactions in each phase is as follows:

(1) Organic phase (cathode): $6Li^{+} + 6e^{-} \rightarrow 6Li^{0}$

(2) Aqueous phase (anode): $3H_2O \rightarrow 3/2O_2 + 6H^{+} + 6e^{-}$

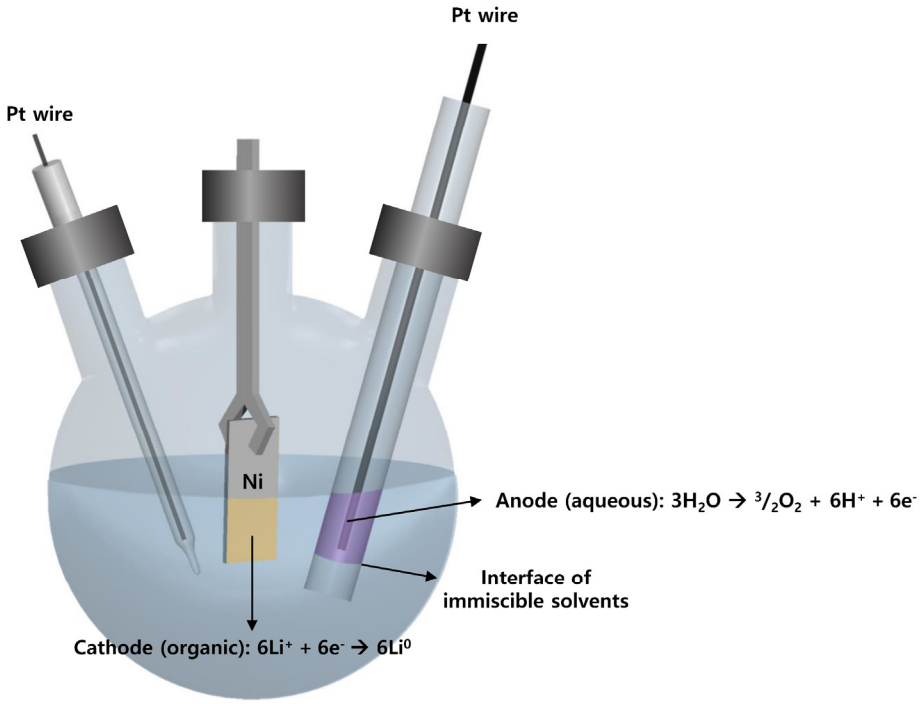

Figure S1. A picture of the electrochemical cell for Li deposition.

Electrochemical measurements: For Li deposition, chronopotentiometry was carried out at a constant current density of 5 mA cm^{-2} (1.25 mA) for 10 min using a potentio/galvanostat (VSP-300 Multi Channels Potentiostat, Biologic) at room temperature. Cyclic voltammetry was carried out in appropriate potential ranges at a scan rate of 10 or 50 mV s^{-1}. Li plating efficiency was measured by dividing the total charges passed before rapid polarization during stripping by the total charges passed during the previous plating using chronopotentiometry (See the caption of Figure S6). Electrochemical impedance spectroscopy (EIS) was carried out in a frequency range from 1 MHz to 0.1 Hz with a potential amplitude of 10 mV.

1.3. Nitridation of Li on Ni substrate ($3Li^{0} + 1/2N_2 \rightarrow Li_3N$)

The Ni substrate with Li deposit was first washed with 2Me-THF, and then transferred to a 125 ml Erlenmeyer flask in a manner that the deposited Li side is facing upward (Figure S2). The bottom of the flask was placed in an oil bath, whose temperature was controlled at a desired temperature level; unless otherwise noted, the temperature was set to 180 °C. Nitridation was carried out by flowing N_2 (UHP, 99.999 %, Airgas) at a flow rate of 600 sccm to provide N_2 atmosphere. Control experiments were also carried out either using pure argon to see the effect of feeding gas, or under N_2 with Ni substrate without Li deposit.

Figure S2. A picture of Li deposit on Ni substrate in an Erlenmeyer flask during nitridation.

1.4. Reaction of Li_3N with acid ($Li_3N + 3H^+ \rightarrow NH_3 + 3Li^+$)

50 ml of 0.1 M H_2SO_4 solution was then poured into the flask to give rise to the final reaction between the solid Li_3N and protons. This reaction is very fast, as could be confirmed from the surface of Ni foil instantaneously and completely washed and thus clean Ni surface was regenerated immediately after the reaction (Figure S3). The acidic solution then contained synthesized NH_3 in the form of NH_4^+, and together with Li^+ ion which can be recycled as a Li^+ source in the anolyte of the Li deposition cell for the next cycle.

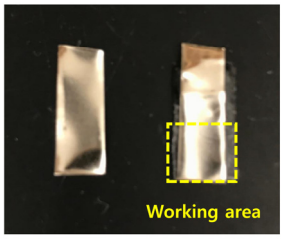

Figure S3. A picture of pristine Ni substrate (left) and regenerated Ni after the reaction between Li_3N and acid (right).

1.5. Calculation of NH_3 synthesis rate and Faradaic efficiency

NH_3 synthesis rate (in mol sec^{-1} cm^{-2}) was calculated according to the following equation:

$$\text{Synthesis rate} = \frac{Amount\ of\ NH_3\ (mol)}{Working\ area\ (cm^2) \times (duration\ of\ Li\ deposition + nitridation)\ (\text{sec})}$$

The Faradaic efficiency for NH_3 synthesis was calculated based on the equation below:

$$\text{FE} = \frac{Amount\ of\ NH_3\ (mol) \times 96485(\frac{C}{mol\ e^-})}{Current\ (A) \times duration\ of\ plating\ (\text{sec}) \times \frac{1\ mol\ Li^0}{1\ mol\ e^-} \times \frac{1\ mol\ NH_3}{3\ mol\ Li^0}}$$

2. Analytical methods

2.1. Quantification of NH_3

The synthesized NH_3 in the 0.1 M H_2SO_4 solution was quantified using spectrophotometry by indophenol blue method. In the spectrophotometric analysis, three reagents were prepared:

(a) Coloring solution: 0.4 M $C_7H_5NaO_3$ (sodium salicylate) + 0.32 M NaOH;

(b)Oxidation solution: 0.75 M NaOH in 10 ml NaOCl (sodium hypochlorite solution, available chlorine 4.00-4.99 %);

(c) Catalyst solution: 0.1 g $Na_2[Fe(CN)_5NO]\cdot 2H_2O$ (sodium nitroferricyanide dihydrate) diluted to 10 ml de-ionized water.

4 ml of the sample was taken from 0.1 M H_2SO_4 containing NH_4^+. Afterwards, pH was adjusted to 13 using 6 M NaOH. Then, 50 µL of oxidizing solution, 500 µL of coloring solution, and 50 µL of catalyst solution were added in a sequential manner to the sample, followed by a quick sonication to mix the reagents. Considering that the absorbance reached a stable plateau after 6000 sec (Figure S4(a)), the absorbance for every sample was measured after 2 hr at a wavelength of 665 nm using a UV-vis spectrophotometer (Shimadzu UV 2700). The same procedure was also applied for several standard solutions to create a calibration curve (Figure S4(b-c)).

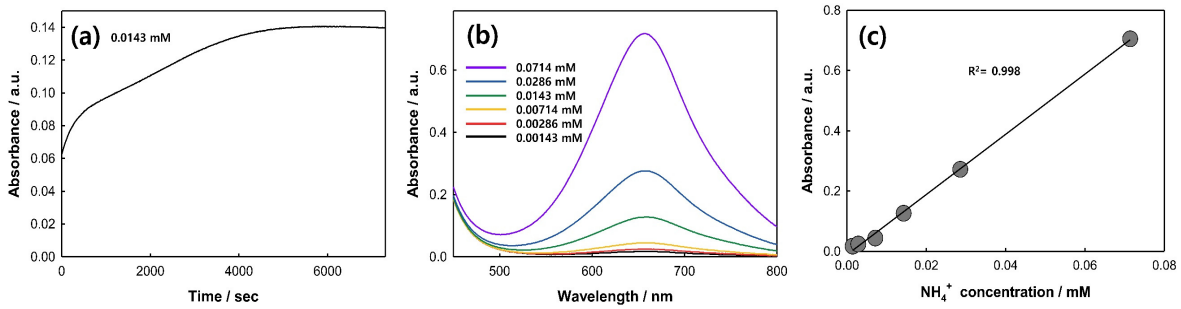

Figure S4. (a) The kinetics of indophenol reagents. The evolution of absorbance at 665 nm measured from a standard solution in the presence of 0.0143 mM of NH_4^+; (b) UV-vis absorption spectra and (c) corresponding calibration curves for colorimetric NH_3 assay using the indophenol blue method.

2.2 Other characterizations

Karl-Fischer titration. Water contamination in the organic phase was determined using Karl-Fischer titration method. Two samples were taken from random spots of the organic electrolytes (without or with 1 wt.% PMMA) after storage times of 0 and 48 hours, respectively. Karl-Fischer titration was then carried out using a Metrohm 831 Karl Fischer 60 coulometer and duplicated for each sample. Before analysis, the coulometer was calibrated using 1000 ppm water standard. The results are shown in Table S1.

Scanning electron microscopy (SEM). The microstructure of the Li deposit was observed by field-emission scanning electron microscopy (FEI Quanta-250). Due to the air-sensitive nature of metallic Li, the Li deposit specimens were mounted on the holders inside a specially designed sample transfer case in a N_2-filled glove box, followed by evacuation using a mechanical pump. A one-way valve and rubber O-ring help ensure a long-time vacuum-tight seal in the case. The case was then transferred into the SEM chamber, and the lid opened automatically during chamber evacuation with the aid of a spring.[2]

Attenuated total reflection-Fourier transform infrared spectroscopy (ATR-FTIR). FT-IR measurements were performed on a Cary 630 FT-IR Spectrometer equipped with a diamond ATR sampling accessory to analyze the deposited species on the Ni substrates. After different stages of charging during the chronopotentiometry, the electrodes were taken out and rinsed immediately by wiping with a piece of tissue paper to remove the remainder of the electrolyte solvent and excess PMMA, followed by drying out in a N_2-filled glove box.[3] The spectra were recorded between 400 and 4000 cm^{-1} with a resolution of 2 cm^{-1}.

X-ray photoelectron spectroscopy (XPS). XPS was carried out on a Kratos Amicus/ESCA 3400 X-ray Photoelectron Spectrometer with Mg Kα X-ray (1253.7 eV photon energy). All spectra were calibrated with the C 1s peak at 284.8 eV. For the Li_3N-deposited Ni substrate, an Ar^+ sputter etching for a total of 640 seconds was performed prior to spectrum collection to remove the surface impurities. All other specimens were prepared in the same way as the ATR-FTIR samples.

^{1}H Nuclear magnetic resonance (^{1}H NMR). ^{1}H NMR characterization of the $^{15}N_2$ isotope experiment was performed on a Bruker Avance NEO 400. The NMR samples were prepared by mixing 0.8 mL of the product solutions containing 0.1 M H_2SO_4 and certain concentrations of NH_4^+ with 0.2 mL of d6-DMSO[4]. To track the nitrogen source of produced NH_3 quantitatively, standard solutions with 5, 10, 25, 50, 75 μM of $^{15}NH_4Cl$ were prepared in 0.1 M H_2SO_4 medium with a known amount of LiOH added.[5] The amount of LiOH was determined from the charge balance of Li deposition. Water suppression and 2000 scans were carried out for all NMR measurements.[6]

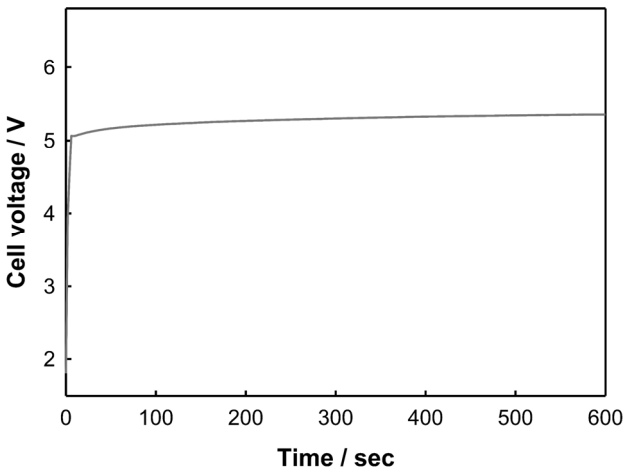

Figure S5. A cell voltage-time curve for the membrane-free aqueous/organic hybrid electrolyte cell at 25 °C (Anode: Pt wire, cathode: Ni foil, anolyte: aqueous 1 M $LiClO_4$, catholyte: 1 M $LiClO_4$/PC + 1wt.% PMMA, current density: 5 mA cm^{-2})

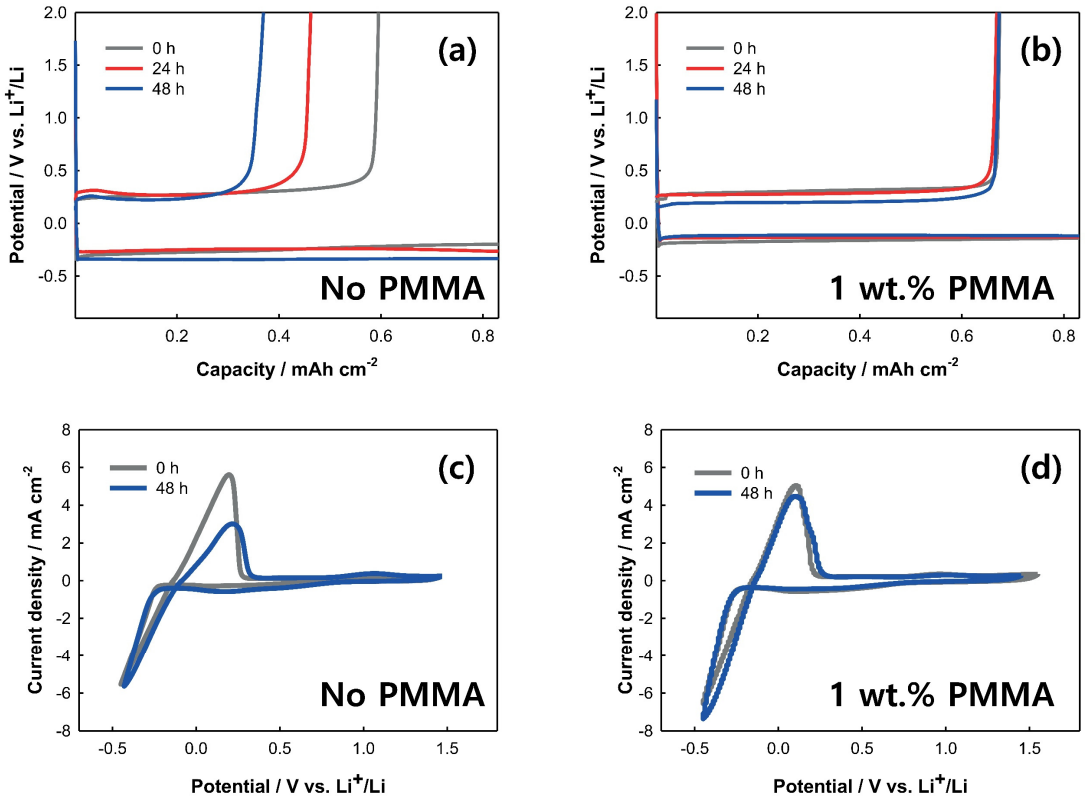

Figure S6. (a, b) Voltage profiles during Li plating and stripping (a) without and (b) with 1 wt.% PMMA after storage times of 0, 24, and 48 hours. The current density during plating/stripping was 5 mA cm^{-2}, and the capacity of Li deposition was 0.83 mAh cm^{-2}. The Li plating efficiency was calculated by dividing the total charges passed before rapid polarization during stripping by the total charged passed during the previous pating.[7]

(c, d) Cyclic voltammetry of Ni foil in 1 M $LiClO_4$/PC (c) without and (d) with 1 wt.% PMMA after storage times of 0 and 48 hours. A scan rate of 50 mV s^{-1} was applied, and the fifth cycle of each voltammogram was taken. The diminished peak of oxidative Li stripping after 48 hours without PMMA clearly shows increased irreversible loss in Li plating. On the other hand, the original oxidation peak was retained in the presence of 1 wt.% PMMA even after 48 hours, implying that more metallic Li could survive with high Coulombic efficiency in the presence of PMMA. This could be ascribed to the inhibition of water diffusion from aqueous to organic phase, as described in Figure 3.

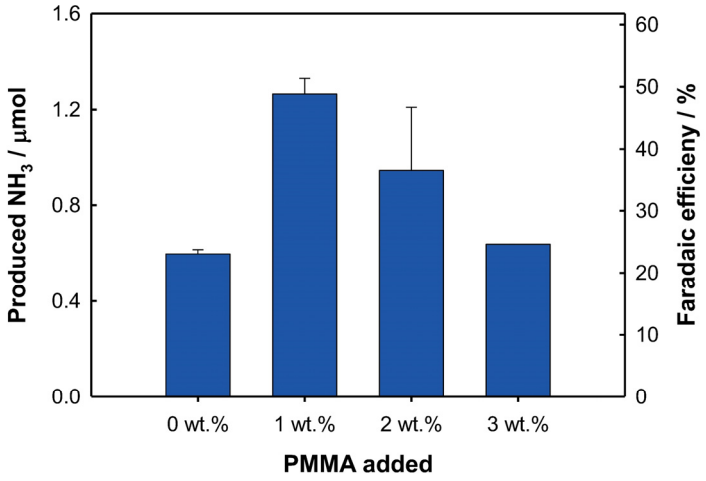

Figure S7. The effect of PMMA content in the organic electrolyte (1 M $LiClO_4$/PC) on the amounts of produced NH_3 and corresponding FEs (capacity: 0.83 mAh cm^{-2}, Li^0 was nitrided at 180 °C for 1 h)

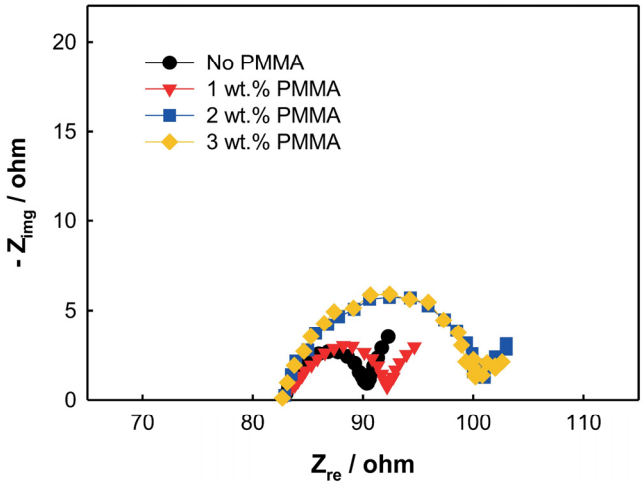

Figure S8. The Nyquist plots of the three-electrode electrochemical cell with various PMMA concentrations in 1 M $LiClO_4$/PC (Li capacity: 0.83 mAh cm^{-2}).

The real part of the impedance at the highest frequency represents the bulk resistance of an electrolyte, and the diameter of a semicircle is an indicator of passive film impedance.[8-10] The width of the semicircle for the organic electrolytes with the addition of 2 and 3 wt.% PMMA was greatly larger than 0 and 1 wt.% PMMA. This increase in the interfacial resistance could be ascribed primarily to the formation of thicker passivation layer with higher PMMA concentrations, which eventually hinders N_2 penetration.[11]

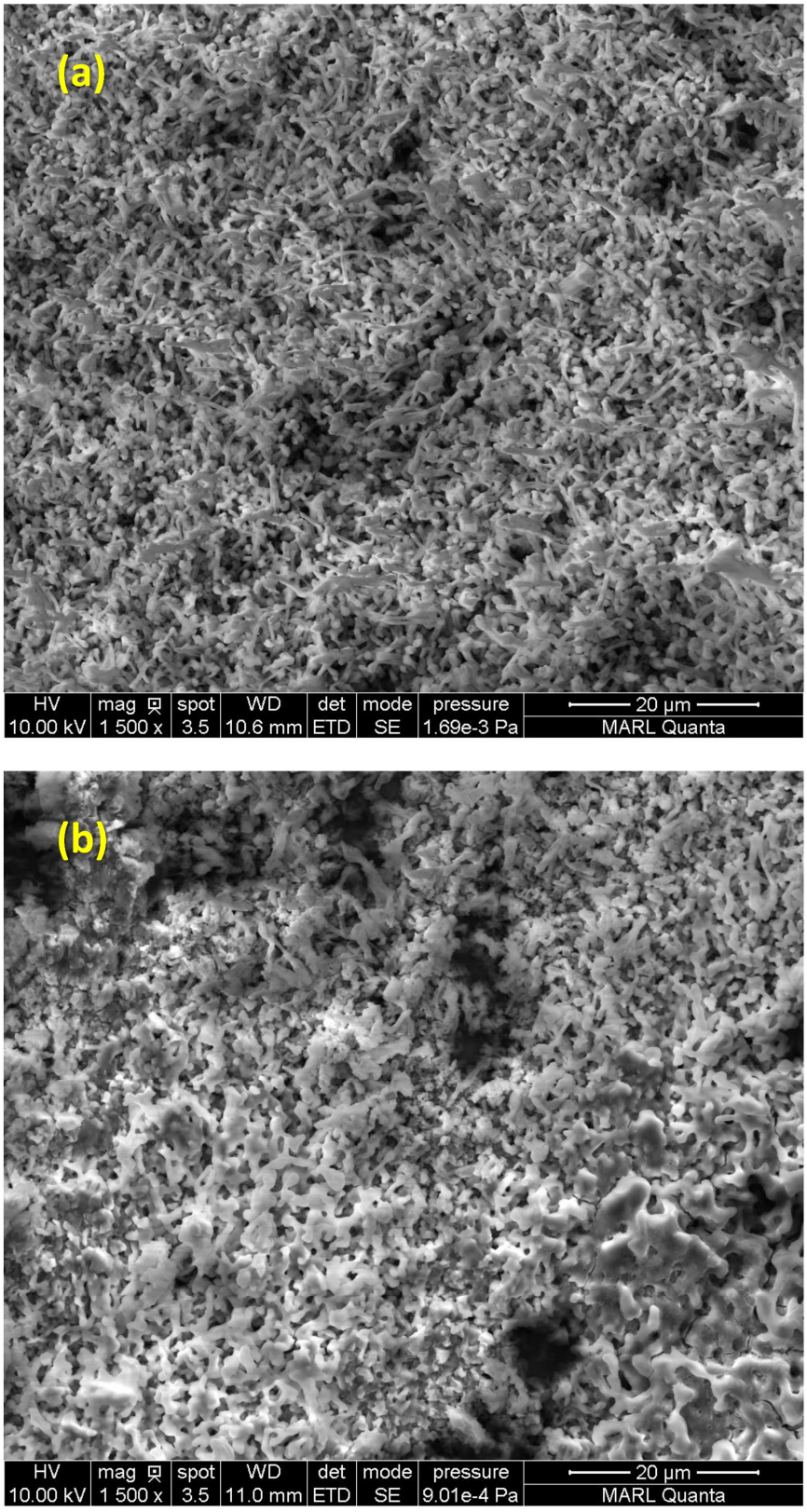

Figure S9. Low magnification SEM images of Li deposited over Ni foils (a) in the absence and (b) presence of 1 wt.% PMMA (Deposition current density: 5 mA cm^{-2} Li capacity: 0.83 mAh cm^{-2}).

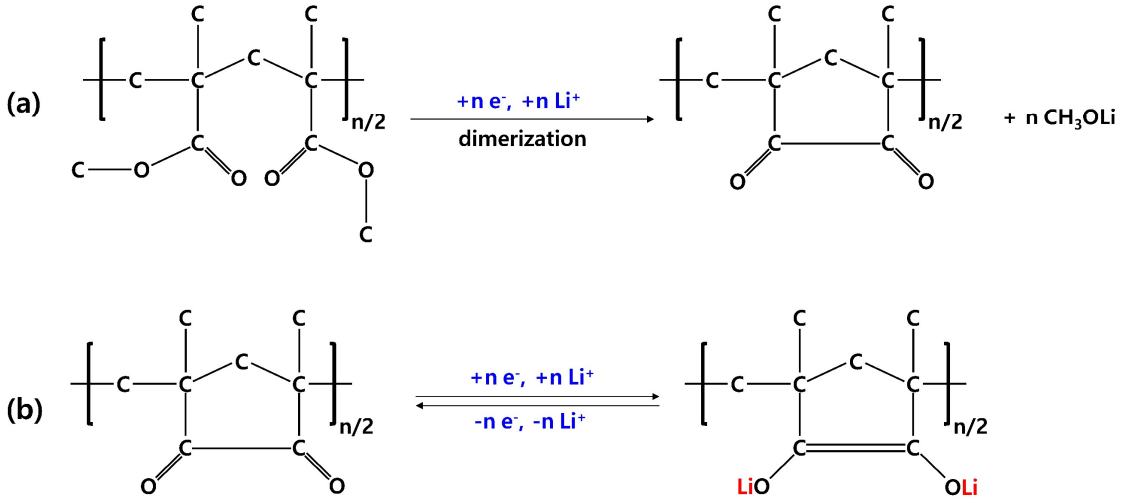

Figure S10. Chemical structures and mechanism showing: (a) irreversible ring-closing reaction forming intramolecular cyclopentanedione and lithium methoxide; (b) reversible lithiation and delithiation process occurring on newly formed carbonyl groups.[12]

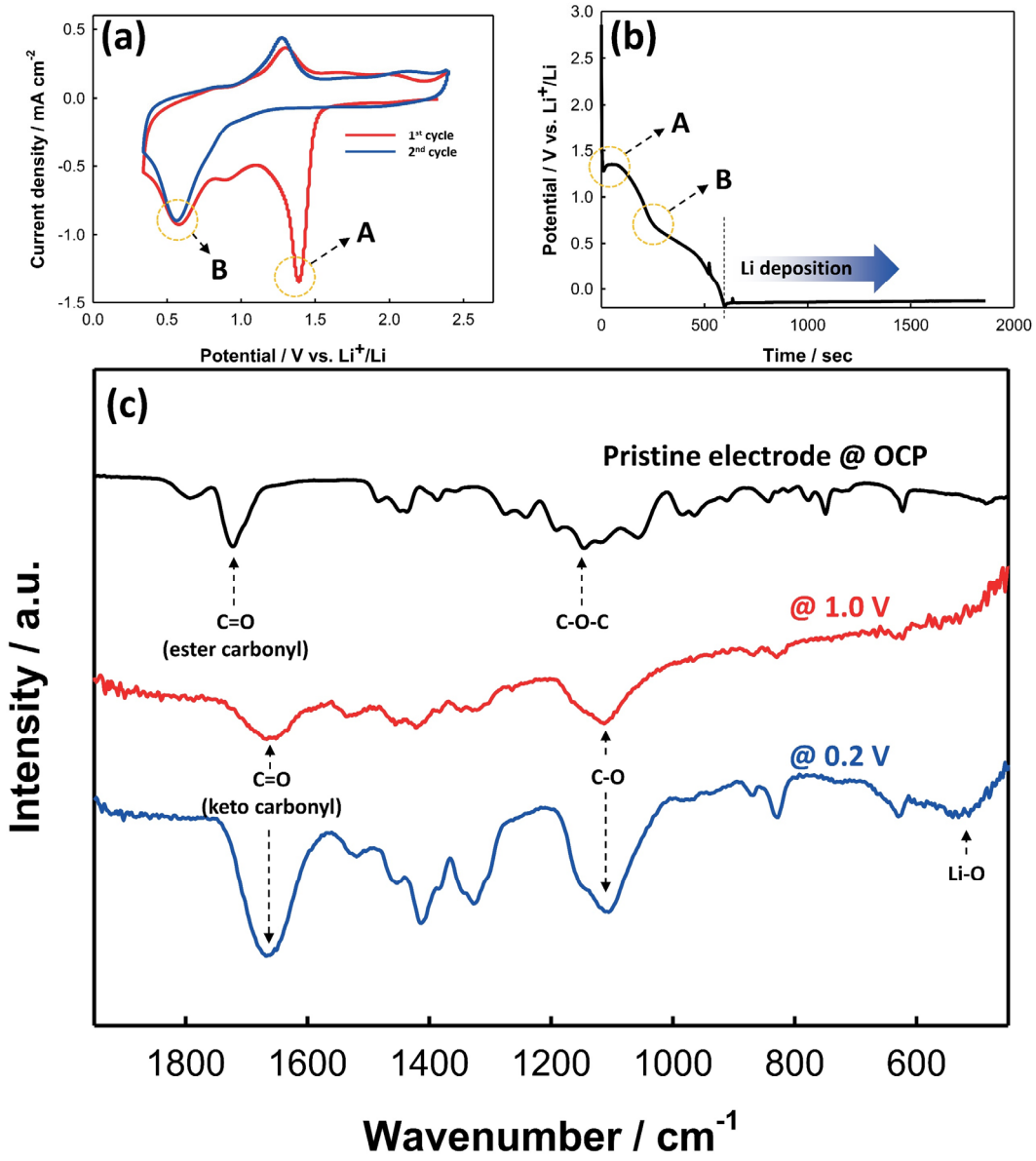

Figure S11. (a) Cyclic voltammetry of Ni substrate in 1 M $LiClO_4$/PC + 1 wt.% PMMA at a scan rate of 10 mV s^{-1} in the potential range of 0.35 ~ 2.4 V (vs. Li^+/Li); (b) A voltage profile during chronopotentiometry at a current density of 0.05 mA cm^{-2}; (c) FT-IR spectra of the surface species on Ni substrates obtained at different stages of charging (black: pristine, red: charged to 1.0 V, blue: charged to 0.2 V (vs. Li^+/Li)).

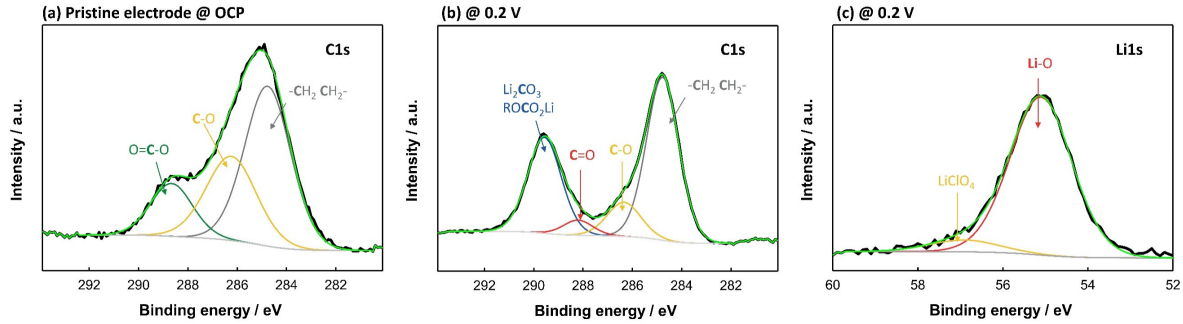

Figure S12. XPS spectra of the surface on Ni substrates obtained at different stages of charging. (a) C1s spectrum of the pristine electrode; (b) C1s spectrum of Ni substrate charged to 0.2 V; (c) Li1s spectrum of Ni substrate charged to 0.2 V (vs. Li^+/Li).

The fitting of C1s spectrum of the pristine electrode at OCP (Figure S12(a)) exhibited two peaks with the binding energies of 286.3 and 288.6 eV, which can be assigned to the methoxyl carbon (C-O) and ester carbonyl carbon (O=C-O).[12] For the electrode charged to 0.2 V (Figure S12(b)), C-O peak weakened, and a new peak was observed at 288.1 eV, which is an indicator of keto carbonyl carbon (C=O).[13-15] Along with Li1s spectrum showing the emergence of Li bound to O (Figure S12(c))[16], this XPS analysis provides supportive evidences of the electrochemical reduction processes described in Figure S10 and S11 and proves the role of PMMA as a storage medium for Li-ions.

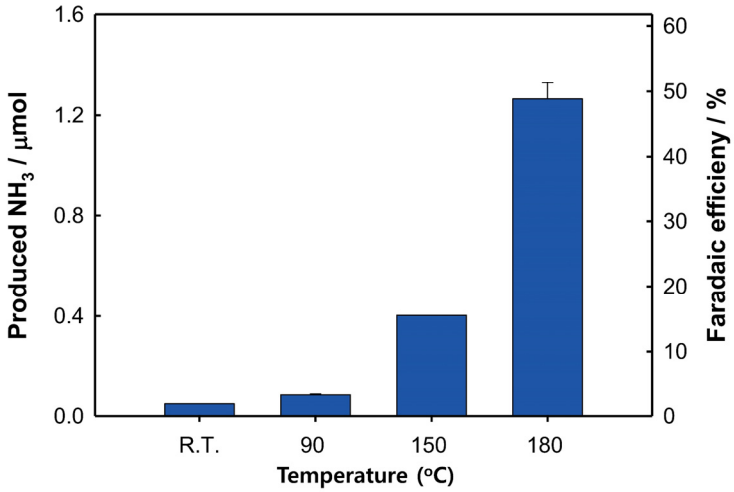

Figure S13. The amount of produced NH_3 and corresponding FEs using Li deposited in 1 M $LiClO_4$/PC + 1 wt.% PMMA nitrided at various temperatures (Li capacity: 0.83 mAh cm^{-2}, Li was nitrided for 1 h).

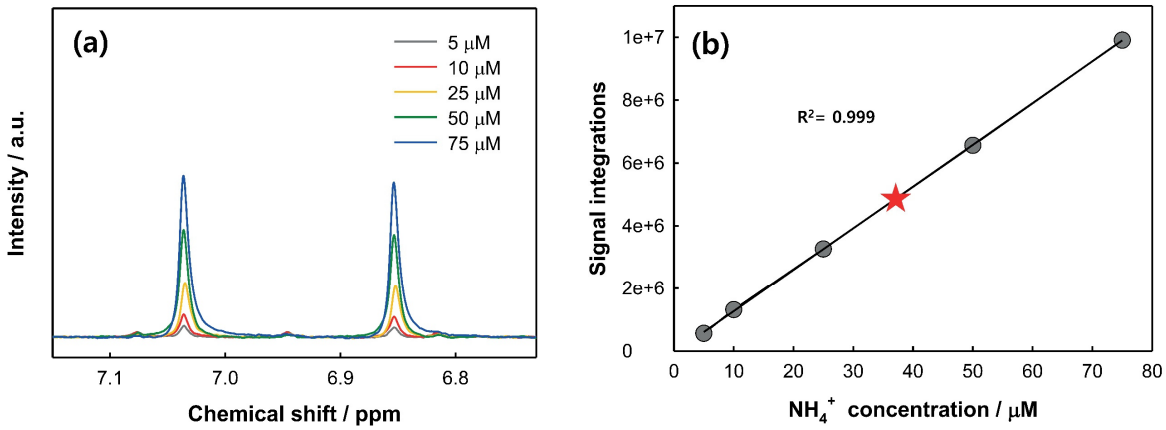

Figure S14. (a) ^{1}H NMR spectra of standard $^{15}NH_4Cl$ solutions with the $^{15}NH_4^+$ concentrations of 5, 10, 25, 70, 75 μM; and (b) corresponding calibration curve from ^{1}H NMR signals in Figure S14(a). The gray circles indicate the concentrations and NMR signal integrations for the standard solutions, which provide a standard calibration line with R^2 value of 0.999. The red star indicates the concentration of $^{15}NH_4^+$ in our sulfuric acid sample after the hydrolysis of Li_3N, which was prepared from the nitridation of metallic Li under $^{15}N_2$ atmosphere. The calculated concentrations of $^{15}NH_4^+$ was 37.1 μM, and this is close to the corresponding value (36.6 μM) determined using the colorimetric indophenol blue method, confirming the reliability of our quantification method.

Table S1. The results of Karl-Fischer analysis

Sample Number	Sample name	Mass /g	Water content / ppm
1	1000 ppm standard	0.102	964.0
2	1000 ppm standard	0.231	1021.0
3	No PMMA #1 - 0 hr - A	0.119	43.2
4	No PMMA #1 - 0 hr - B	0.270	50.8
5	No PMMA #2 - 0 hr - A	0.227	50.4
6	No PMMA #2 - 0 hr - B	0.431	50.4
7	1wt.% PMMA # 1 - 0 hr - A	0.281	55.5
8	1wt.% PMMA # 1 - 0 hr - B	0.386	55.6
9	1wt.% PMMA # 2 - 0 hr - A	0.276	71.3
10	1wt.% PMMA # 2 - 0 hr - B	0.570	71.6
11	No PMMA #1 - 48 hr - A	0.293	2912.0
12	No PMMA #1 - 48 hr - B	0.189	2877.9
13	No PMMA #2 - 48 hr - A	0.227	20116.0
14	No PMMA #2 - 48 hr - B	0.431	20114.2
15	1wt.% PMMA # 1 - 48 hr - A	0.281	721.0
16	1wt.% PMMA # 1 - 48 hr - B	0.386	715.0
17	1wt.% PMMA # 2 - 48 hr - A	0.276	792.1
18	1wt.% PMMA # 2 - 48 hr - B	0.570	428.0

Table S2. Experimental studies and results of the state-of-the-art NH_3 electro-synthesis

Reference	Catalyst/cathode material	Electrolyte system	NH_3 production rate ($mol/cm^2 \cdot s$)	Faradaic efficiency (%)
Energy Environ. Sci. 2017, 10, 2516.	Fe/F-doped SnO_2	Ionic liquid	2.3×10^{-11}	60
Electrochim. Acta. 2005, 50, 5423.	Ni	LiCl-KCl-CsCl-Li_3N eutectic (400°C)	2.0×10^{-8}	23
Science. 2014, 345, 637.	Nano-Fe_2O_3	Molten NaOH/KOH	2.4×10^{-9}	35
Energy Environ. Sci. 2017, 10, 1621.	Steel	LiCl-KCl/LiOH-LiCl molten salt (450°C)	9.2×10^{-9}	89
Chem. Sus. Chem. 2018, 11, 120.	Ni	Aqueous/LISICON/ organic electrolyte	1.9×10^{-9}	50
Nat. Commun. 2018, 9, 3485.	B_4C nanosheet	0.1 M HCl	4.3×10^{-11}	16.0
Nat. Commun. 2018, 9, 1795.	Pd/C	0.1 M PBS	9.6×10^{-12}	8.2
ACS Energy Lett. 2019, 4, 430	Ru/MoS2	0.01 M HCl	1.1×10^{-10}	17.6
Adv. Mater. 2017, 29, 1604799.	Au nanorods	0.1 M KOH	2.7×10^{-11}	4.0
J. Am. Chem. Soc. 2018, 140, 13387	VN	Nafion-based flow cell	3.3×10^{-10}	6.0
Angew. Chem. Int. Ed. 2019, 58, 2321.	Mo/N-doped porous carbon	0.1 M KOH	2.2×10^{-10}	14.6
ACS Catal. 2019, 9, 2902	Bi nanosheet	0.1 M Na_2SO_4	4.2×10^{-11}	10.5
This work	**Ni**	**Aqueous/organic hybrid electrolyte**	$\mathbf{1.2\times10^{-9}}$	**57**

References:

[1] Y.-C. Lu, H. A. Gasteiger, E. Crumlin, R. McGuire and Y. Shao-Horn, Journal of The Electrochemical Society, 2010, 157, A1016.

[2] M. S. Ding, S. L. Koch and S. Passerini, Electrochimica Acta, 2017, 240, 408–414.

[3] G. V. Zhuang, H. Yang, B. Blizanac and P. N. Ross, Electrochemical and Solid-State Letters, 2005, 8, A441.

[4] J. Liu, M. S. Kelley, W. Wu, A. Banerjee, A. P. Douvalis, J. Wu, Y. Zhang, G. C. Schatz and M. G. Kanatzidis, Proceedings of the National Academy of Sciences, 2016, 113, 5530–5535.

[5] L. Han, X. Liu, J. Chen, R. Lin, H. Liu, F. Lü, S. Bak, Z. Liang, S. Zhao, E. Stavitski, J. Luo, R. R. Adzic and H. L. Xin, Angewandte Chemie International Edition, 2019, 58, 2321–2325.

[6] F. Zhou, L. M. Azofra, M. Ali, M. Kar, A. N. Simonov, C. McDonnell-Worth, C. Sun, X. Zhang and D. R. MacFarlane, Energy & Environ. Sci., 2017, 10, 2516-2520

[7] R. Selim and P. Bro, Journal of The Electrochemical Society, 1974, 121, 1457.

[8] Q. Lu, J. Yang, W. Lu, J. Wang and Y. Nuli, Electrochimica Acta, 2015, 152, 489–495.

[9] D. Lin, J. Zhao, J. Sun, H. Yao, Y. Liu, K. Yan and Y. Cui, Proceedings of the National Academy of Sciences, 2017, 114, 4613–4618.

[10] B. Wu, X. Chen, C. Zhang, D. Mu and F. Wu, New Journal of Chemistry, 2012, 36, 2140.

[11] C. Tang, Y. Ren, Z. Chen and J. Ding, Ionics, 2019, 25, 1007–1014.

[12] Y. Wang, L. Zhang, L. Zhang, F. Zhang, P. He, H. Zheng and H. Zhou, Advanced Energy Materials, 2016, 6, 1601375.

[13] X. Feng, N. Dementev, W. Feng, R. Vidic and E. Borguet, Carbon, 2006, 44, 1203–1209.

[14] Q. Yang, Z. Wang and J. Weng, Soft Matter, 2012, 8, 9855.

[15] Z. Zhang, S. Liu, J. Xiao and S. Wang, Journal of Materials Chemistry A, 2016, 4, 9691–9699.

[16] N. Togasaki, R. Shibamura, T. Naruse, T. Momma and T. Osaka, APL Materials, 2018, 6, 047704.